CHAPTER 6

Effect of USSP on Low Cycle Fatigue Behaviour

6.1 INTRODUCTION

In this chapter, the influence of ultrasonic shot peening (USSP240) as well that of stress-relieving at 400°C, following the ultrasonic shot peening (USSP240-SR), on the low cycle fatigue life of the Ti-13Nb-13Zr alloy, was investigated at room temperature. The results are discussed in terms of increase in the resistance of the material against crack initiation due to grain refinement in the surface region and the associated compressive residual stresses resulting from USSP treatment. Fatigue samples were prepared from the heat-treated blanks (900°C solution treated and quenched in water) and gauge section was mechanically polished with emery papers up to 2500 grit size to remove machining marks, and final polishing was done using 0.5 μm alumina powder suspension in water as abrasive. The polished gauge surface of fatigue samples was subjected to uniform USSP treatment with hard steel balls of 3 mm diameter for 120, 240 and 360 s of USSP duration by rotating the sample to ensure uniform peening along the circumference of the cylindrical gauge section and were designated as USSP120, USSP240 and USSP360 respectively. Total strain controlled low cycle fatigue (LCF) tests were conducted with fully reversible (R = -1) axial loading, with triangular waveform, at total strain amplitudes of ±0.55%, ±0.60%, ±0.70%, ±0.80%, and ±0.90%, at a fixed strain rate of 0.005 s^{-1}. The microstructure and fracture morphology of the fatigue tested specimens were analyzed using scanning electron microscope at 30 kV.

The Un-USSP, USSP240 and USSP240-SR samples were characterized for their microstructure, surface roughness, hardness and low cycle fatigue behaviour. The near

surface region of the USSP240 specimen was associated with high level of compressive residual stress, whereas there was much lower compressive stress in surface region of the USSP240-SR specimen. The fatigue life of the material was significantly enhanced three times due to USSP240; however, it was slightly lowered following the stress-relieving treatment but was higher than that of the Un-USSP.

NOTE: In study related to Fatigue behaviour, we have used higher duration of USSP treatment (120, 240 and 360 s for samples) for developing greater depth of modified layer that will prevent crack initiation and thereby helps in improving the fatigue life.

6.2 MICROSTRUCTURE

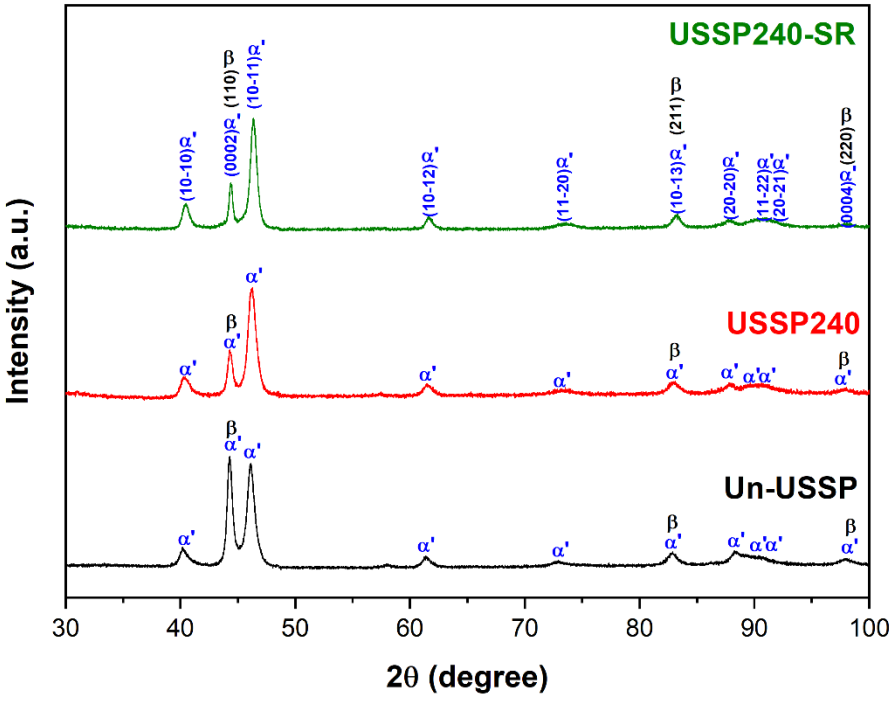

Figure 6.1 XRD peaks of the Un-USSP, USSP240 and USSP240-SR samples.

The XRD peaks of Un-USSP240, USSP240 and USSP240-SR samples shown in Figure 6.1 revealed that the microstructure consists of only two phases α′ and β in all the three conditions; thus, no phase transformation was observed following the USSP240

and USSP240-SR treatments. However, there is decrease in volume fraction of the β phase, following the USSP240 treatment, as indicated by decrease in the intensity of β (110) and (211) peaks. The diffraction peaks of the Un-USSP sample are apparently broadened after the USSP, that indicates surface grain refinement and increase in atomic level lattice strains. The broadening of the XRD peaks can be associated with the combined effect of grain refinement, lattice-strain and instrumental broadening. The USSP240-SR sample also showed some broadening in peaks.

6.3 ROUGHNESS

Table 6.1 shows average surface roughness of the fatigue samples subjected to various durations of USSP. Surface roughness of the Un-USSP sample is significantly lower than the samples subjected to USSP240 and USSP240-SR treatments. The high roughness in the USSP treated samples is attributed to much uneven surface, caused by the impacts of hard steel shots of 3 mm diameter during the USSP treatment. Similar roughness was also observed in the USSP240-SR samples.

Table 6.1 Surface roughness* of the Un-USSP, USSP240 and USSP240-SR treated specimens.

Treatment Conditions	**R_a (µm)**	**R_q (µm)**	**R_z (µm)**
Un-USSP	0.204±0.038	0.256±0.043	1.347±0.092
USSP240	1.273±0.128	1.563±0.163	6.693±0.643
USSP240-SR	1.394 ±0.161	1.712±0.189	6.868±0.758

*R_a-Arithmetic mean roughness.
*R_q-Root-mean-square (RMS) roughness.
*R_z-Average maximum height of roughness.

6.4 MICROHARDNESS

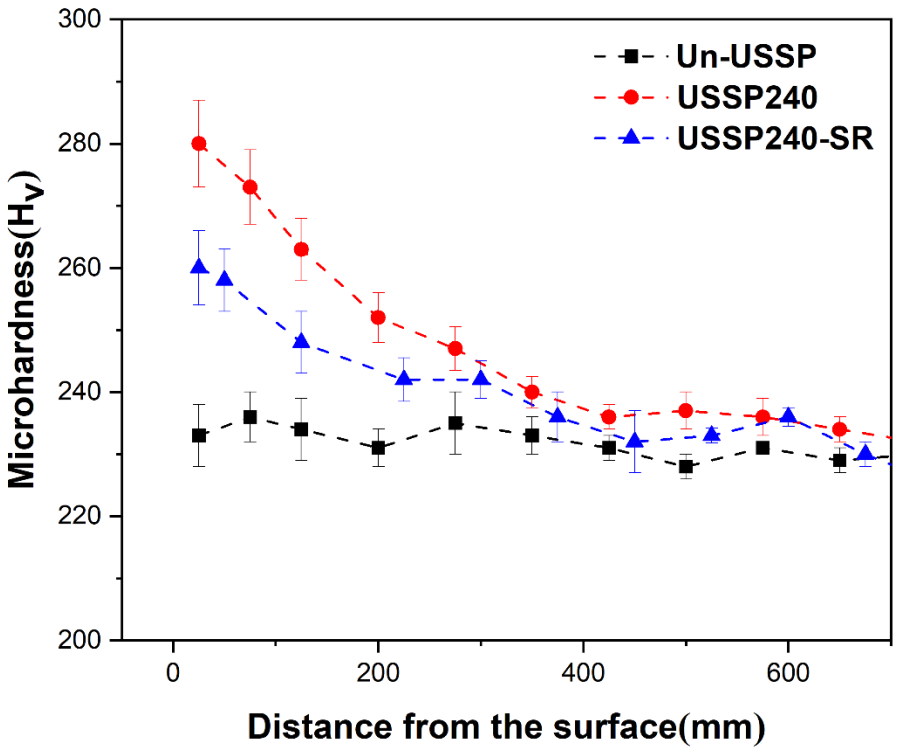

Figure 6.2 Variation of hardness across the depth of Un-USSP, USSP240 (240 seconds) and USSP240-SR samples.

Figure 6.2 shows microhardness profiles of the specimens, following USSP240, along the longitudinal section, normal to the shot-peened surface. It shows the change in microhardness, from the surface to interior. The maximum hardness was observed near the surface, and there was gradual decrease towards the interior. The gradient microstructure, with progressive increase in grain size, and change in residual stress are responsible for the gradual decrease in hardness. The hardness of the un-treated sample was ~233 Hv, while that of the USSP240 treated sample was ~270 Hv. The hardness of the USSP240-SR sample was reduced to ~260 Hv.

6.5 RESIDUAL STRESS

The variation of residual stress from surface towards interior in the USSP240 and USSP240-SR samples is shown in Figure 6.3.

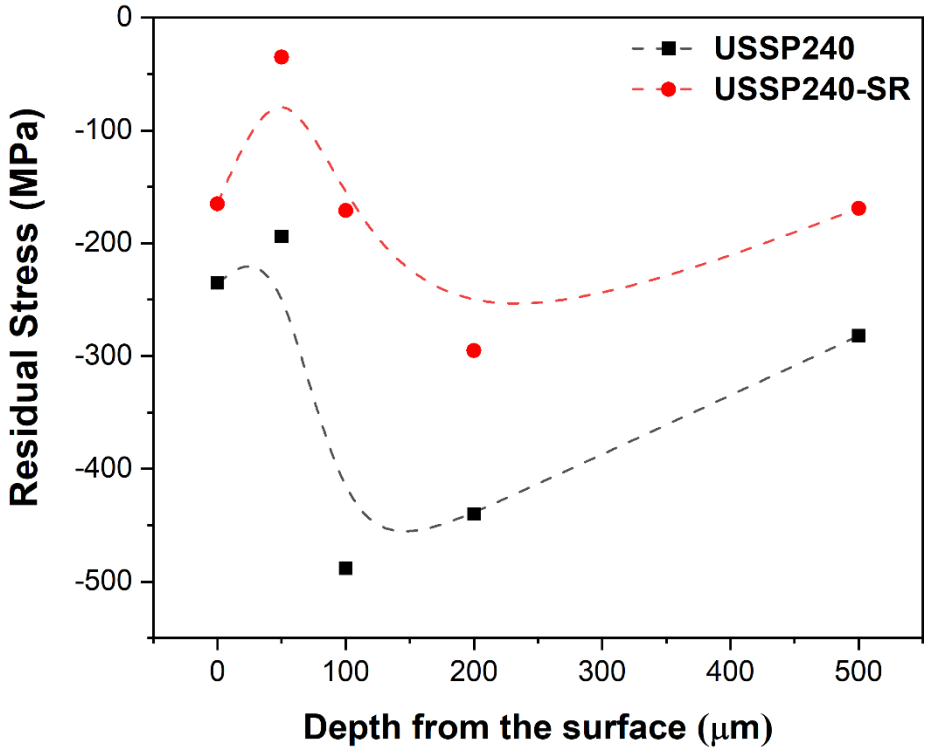

Figure 6.3 Residual stress as a function of depth in USSP240 and USSP240-SR samples.

The residual stress is compressive in nature and found to be maximum at the sub-surface; however, the compressive residual stress is much lower in the stress relieved condition than that in the as shot peened condition. For the USSP240 treated sample the residual stress is –245 MPa at the surface, increased to maximum level of –490 MPa at the depth of 100 μm and decreased to –295 MPa at the depth of 500 μm. On the other hand, in the USSP240-SR sample, it is –170MPa at the surface, decreased to –300 MPa at the depth of 200 μm and decreased to –180 MPa at the depth of 500 μm.

6.6 LOW CYCLE FATIGUE BEHAVIOUR

Table 6.2 shows fatigue life of the specimens in the Un-USSP condition and USSP treated for different durations of 120, 240 and 360 s at a total strain amplitude of ±0.70%. Although fatigue life improvement can be seen in all the USSP treated specimens (USSP120, USSP240, and USSP360), the maximum improvement in fatigue life is there in the specimen USSP treated for 240 s (USSP240).

Table 6.2 Fatigue life of the specimens USSP treated for different durations at $\Delta\varepsilon_t/2=\pm 0.70\%$.

Designation	Fatigue life (cycles)
Un-USSP	16680
USSP120	34358
USSP240	46006
USSP360	38235

These tests were repeated twice to check the reproducibility of data. Thus, the 240 s of USSP treatment was found to exhibit optimum LCF life, hence LCF tests at the different total strain amplitudes from ±0.55% to ±0.90% were conducted for only this condition.

6.6.1 Cyclic Stress Response

The cyclic stress response of the specimens in the Un-USSP, USSP240 and USSP240-SR conditions, at different total strain amplitudes of ±0.55 to ±0.90% are shown in Figures 6.4a, b and c, respectively. Improvement in fatigue life may clearly be seen, following the USSP treatment compared to the Un-USSP. However, fatigue life in the USSP240-SR condition is slightly lowered in comparison with that of the USSP240 condition. There is a trend of rapid but moderate hardening in the beginning for about 50 and 70 cycles, at all the strain amplitudes from ±0.55 to ±0.90%, in the Un-USSP and

USSP240 condition, respectively. The cyclic stress remains more or less constant during the subsequent large number of cycles and drops rapidly at the end, prior to fracture. The degree of cyclic hardening increases with increase in the strain amplitude. The sharp drop in stress at the end is due to rapid crack propagation in the last stage, leading to fracture. In contrast, in the USSP240-SR condition, there is cyclic hardening during the initial cycles and softening in the subsequent large number of cycles, followed by rapid drop during the last stage leading to fracture (Figure 6.4c).

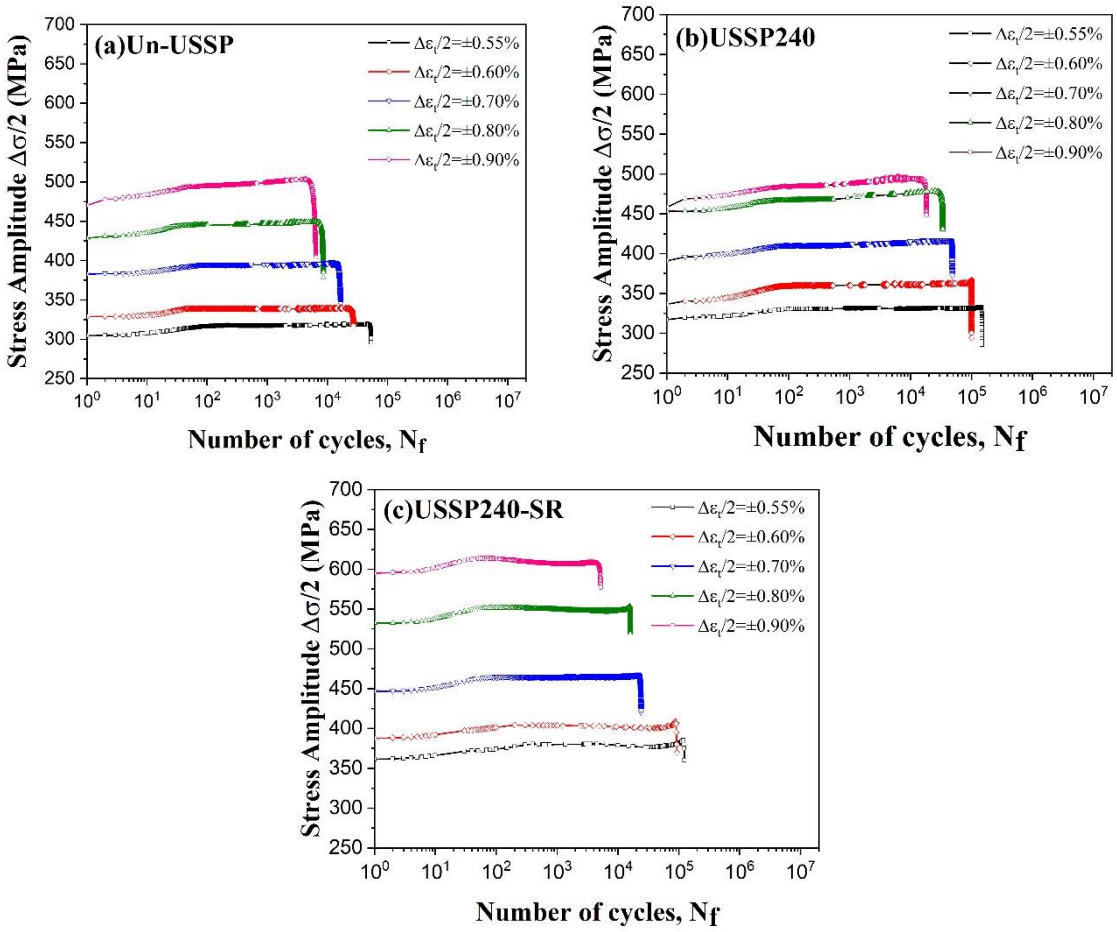

Figure 6.4 Cyclic stress response curves of (a) Un-USSP, (b) USSP240 and (c) USSP240-SR samples.

The number of cycles at the onset of softening is not independent of strain amplitude like that in the Un-USSP and USSP240-SR conditions; rather, strongly dependent on the strain amplitude in the USSP240-SR condition. In the USSP240-SR

conditions, softening occurs at ~800 cycles at ±0.55% and the number of cycles decreases to ~ 50, at the highest strain amplitude of ±0.90%. The degree of softening increases with increase in the strain amplitude.

The cyclic stress level, at all the strain amplitudes, is considerably higher in the USSP240-SR condition as compared to those in the Un-USSP and USSP240 conditions. The higher strength and its effect on lowering of plastic strain in the USSP240-SR condition, in respect of the other two conditions, may be appreciated from the hysteresis loops in the three conditions (Figure 6.5). A substantial increase in fatigue life can be observed in the USSP treated condition (Figure 6.4b) at all the applied total strain amplitudes, with respect to that of the Un-USSP specimens (Figure 6.4a**).**

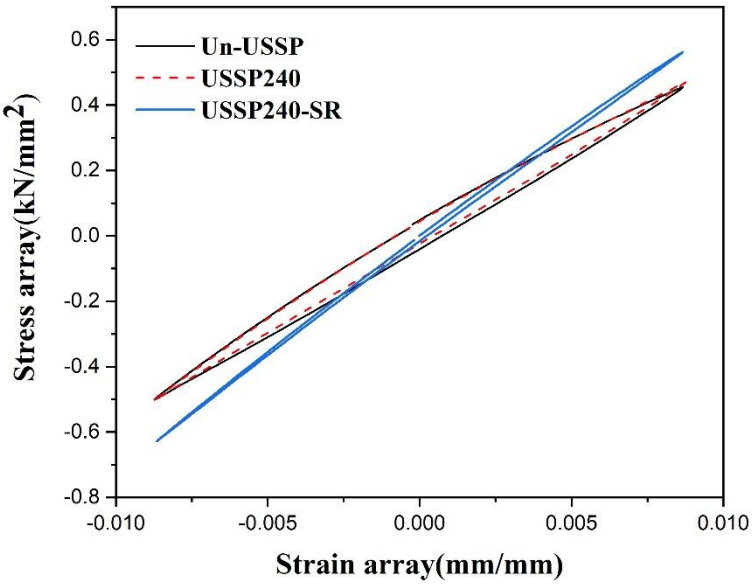

Figure 6.5 Fatigue hysteresis loops for first cycles in the Un-USSP, USSP240 and USSP240-SR conditions.

Fatigue behaviour in the three conditions is analysed by the Coffin-Manson relationship between the plastic strain amplitude ($\Delta\varepsilon_p/2$) and the number of reversals to failure ($2N_f$), as given below [288]:

$$\frac{\Delta\varepsilon_p}{2} = \varepsilon'_f\left(2N_f\right)^c \qquad \text{(Equation 6.1)}$$

Where, ε'_f is fatigue ductility coefficient and c fatigue ductility exponent. The Coffin-Manson (C-M) plots between $\log((\Delta\varepsilon_p/2)$ and $\log(2N_f)$ for the three conditions are displayed in Figure 6.6.

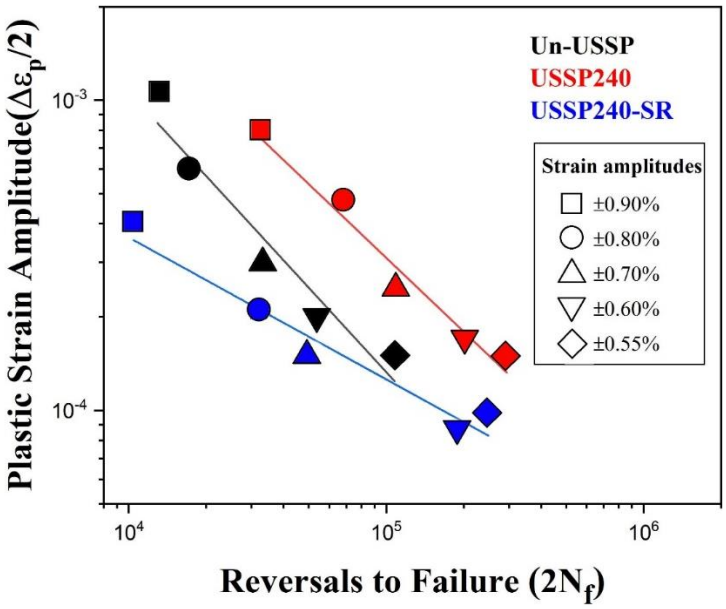

Figure 6.6 Coffin-Manson plot for the Un-USSP, USSP240 and USSP240-SR samples.

Table 6.3 LCF parameters calculated from Coffin-Manson plot for the Un-USSP, USSP240 and USSP240-SR conditions.

Conditions	Fatigue Ductility	
	Coefficient (ε'_f)	Exponent (c)
Un-USSP	4.38	−0.90
USSP240	2.78	−0.80
USSP240-SR	1.07	−0.46

The above parameters were determined from the plots shown in Figure 6.6, and their values are presented in Table 6.3. Low cycle fatigue data are presented in Table 6.4; it may be seen from this table that the plastic strain amplitude, at half fatigue life, is lowest in the USSP240-SR condition, as also seen from the smallest width of the

hysteresis loop in Figure 6.5. It appears from Figure 6.6 that fatigue life is lowest in the USSP240-SR condition; however, fatigue life in this condition is higher than that of the Un-USSP at all the strain amplitudes, except that at the highest strain amplitude of ±0.90% (Table 6.4).

Table 6.4 Low cycle fatigue data in Un-USSP, USSP240 and USSP240-SR conditions of samples at different total strain amplitudes.

Sr. No.	Total Strain Amplitude $\Delta\varepsilon_t/2$ $\times10^{-2}$	Sample Conditions								
		Un-USSP			USSP240			USSP240-SR		
		$\Delta\varepsilon_p/2$ $\times10^{-2}$	$\Delta\varepsilon_e/2$ $\times10^{-2}$	$2N_f$	$\Delta\varepsilon_p/2$ $\times10^{-2}$	$\Delta\varepsilon_e/2$ $\times10^{-2}$	$2N_f$	$\Delta\varepsilon_p/2$ $\times10^{-2}$	$\Delta\varepsilon_e/2$ $\times10^{-2}$	$2N_f$
1	±0.55	0.015	0.535	108000	0.015	0.535	294000	0.010	0.540	249498
2	±0.60	0.020	0.580	54142	0.017	0.583	200720	0.009	0.591	188164
3	±0.70	0.030	0.670	33360	0.025	0.675	97010	0.015	0.685	49420
4	±0.80	0.060	0.740	17198	0.048	0.753	67540	0.021	0.779	31960
5	±0.90	0.105	0.795	12956	0.080	0.820	32320	0.040	0.860	10420

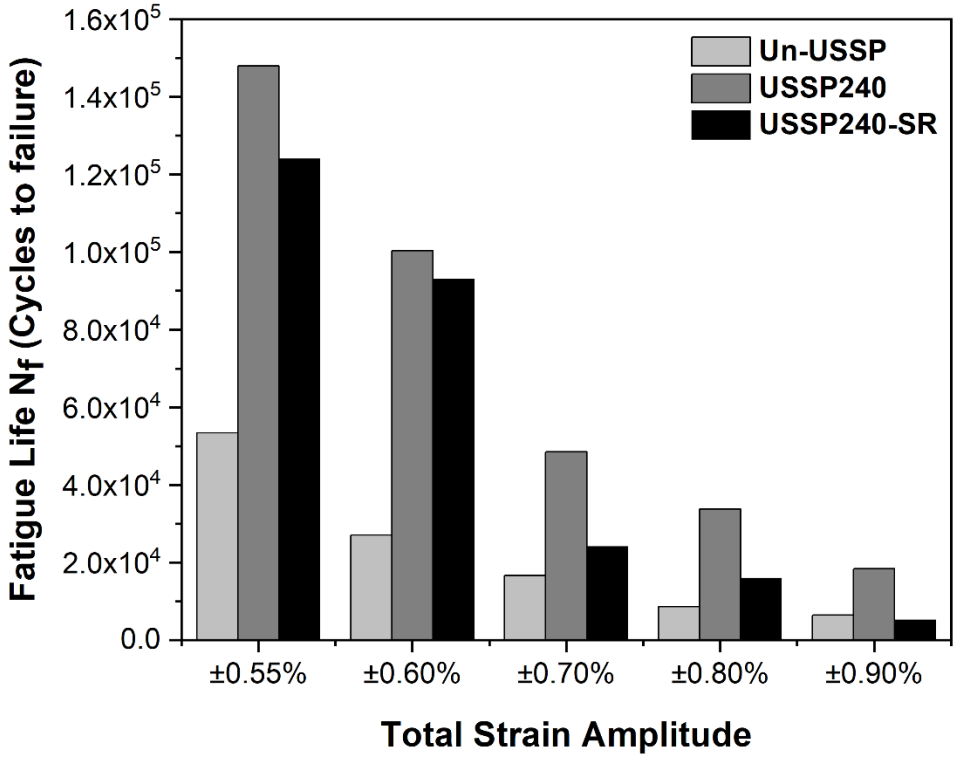

Figure 6.7 Fatigue life cycles for the Un-USSP, USSP240 and USSP240-SR conditions, at different total strain amplitudes.

The lowest level of the C-M plot corresponding to the USSP240-SR condition in Figure 6.6 is due to lowest plastic strain amplitudes in this condition (Table 6.4). The five total strain amplitudes from ±0.55% to ±0.90%, are marked by different symbols, on C-M plots of the three conditions. The lowest fatigue life in the USSP240-SR condition, at the highest strain amplitude of ±0.90%, may be due to early crack initiation from the hardened surface; however, as the strain amplitude decreases, the number of cycles to attain the peak stress increases, this is due to decrease in the number of twins and dislocations, during stress relieving treatment of the USSP240 treated specimens. Fatigue life in the USSP240-SR condition, at the lower strain amplitudes of ±0.60% and ±0.55%, may be seen to be comparable to that of the USSP240 condition (Table 6.4). As shown by the bar diagram in Figure 6.7, presenting fatigue life at different total strain amplitudes, it is evident that fatigue life in the USSP240 condition is enhanced significantly with respect to that of the Un-USSP condition. However, the improvement in fatigue life is relatively less in the USSP240-SR condition than that in the USSP240 condition.

6.6.2 Fracture Characteristics

Fracture surfaces of the Un-USSP, USSP240, and USSP240-SR specimens tested at different total strain amplitudes, from ±0.70% to ±0.90%, are shown in Figures 6.8a to i. The crack initiation sites and crack propagation areas are marked with yellow circles and dashed lines, respectively. Crack initiation in the Un-USSP and USSP240-SR samples was from the outer surface, whereas it was from inside of the USSP240 treated samples. At higher strain amplitudes, the crack initiation was from the region near the surface, however, at the lower strain amplitude it was found to be from the inside. Relatively, larger number of crack initiation sites may be seen in the Un-USSP samples with respect to that in the USSP240-SR samples.

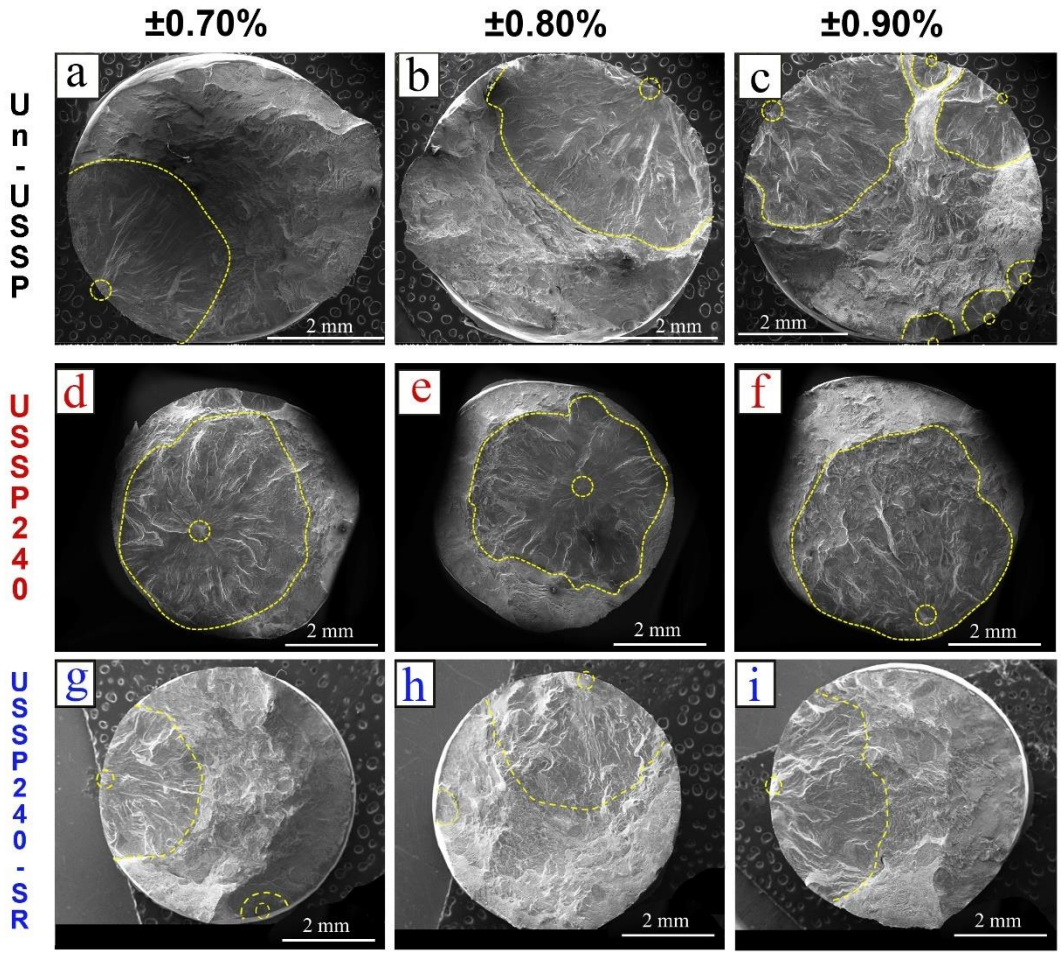

Figure 6.8 SEM micrographs showing fracture surface of Un-USSP, USSP240 treated and USSP-SR samples, at different total strain amplitudes.

Figure 6.9 depicts fatigue striations and micro-cliffs in the region of stable fatigue crack propagation, the yellow arrows indicate the direction of fatigue crack growth (FCG). Crack path may be seen to be more tortuous in the USSP240 treated samples than those in the Un-USSP and USSP240-SR samples. Some secondary cracks may also be seen on fracture surface of the Un-USSP and USSP240-SR specimens. The larger inter-striation spacings on the fracture surface of the Un-USSP fatigue sample (Figures 6.9a-c) than those of the USSP240 treated samples (Figures 6.9d-f) indicate that the rate of crack propagation was higher in the untreated condition.

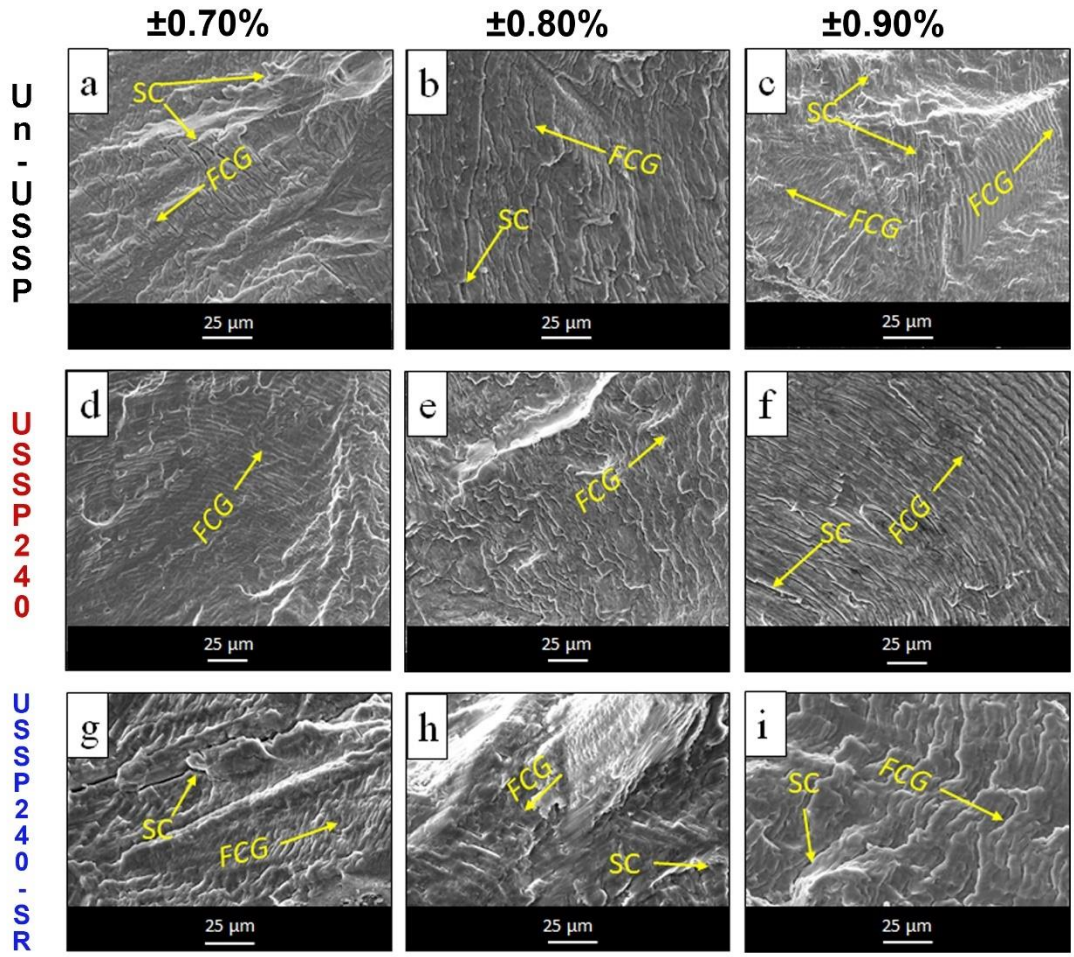

Figure 6.9 SEM micrographs showing fracture surface morphology of Un-USSP, USSP240 treated and USSP240-SR samples, at different total strain amplitudes.

Transmission electron microscopy was used to analyze deformation behaviour of the fatigue tested samples, at total strain amplitude of ±0.70% and TEM micrographs are shown in Figure 6.10 for the Un-USSP, Figures 6.11 & 6.12 for the USSP240 treated, and Figure 6.13 for the USSP240-SR specimens. TEM micrograph revealed that the deformation of this alloy occurs mainly through twinning. Large number of twins can be seen in the fatigue tested specimens. The presence of double diffraction spots in the SAED pattern of the fatigue tested Un-USSP samples, corresponding to the region marked in Figure 6.10b, establishes the occurrence of twinning.

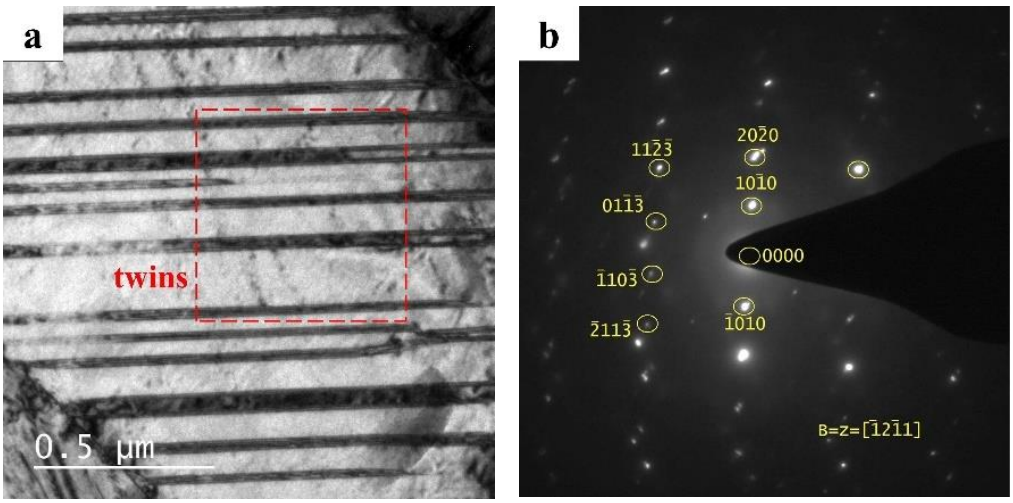

Figure 6.10 TEM images of Un-USSP sample, fatigue tested at ±0.70% strain amplitude showing; (a) α′ laths with twinned region identified by (b) double diffraction spots in SAED pattern

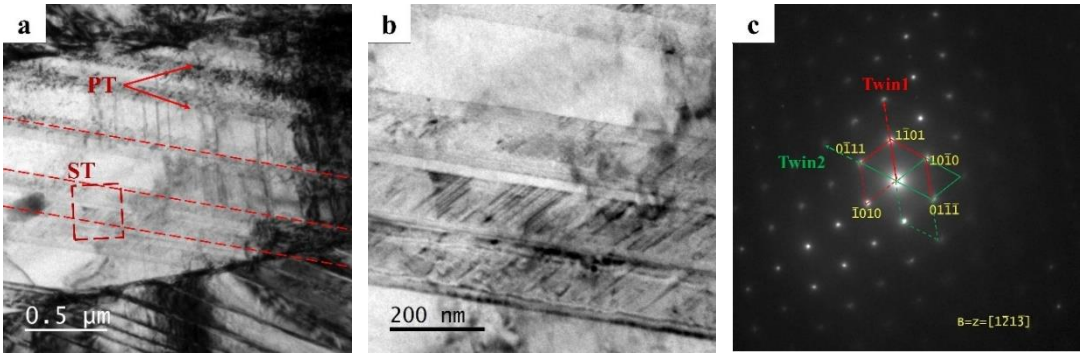

Figure 6.11 TEM images of USSP240 sample, fatigue tested at ±0.70% strain amplitude showing α′ laths having (a) twin variants PT (primary twins) and ST (secondary twins) (b) enlarged view of red marked area and (c) corresponding SAED pattern along the [$1\bar{\mathbf{2}}1\bar{\mathbf{3}}$]α′ zone axis indicating cross twins identified as two twin variants of the {$1\bar{\mathbf{1}}01$} twinning system.

TEM micrographs of the fatigue tested USSP240 samples also showed twin variants of primary twins and secondary twins within micrographs shown in Figures 6.11a and 6.11b. There is lamellar structure of α′ martensite with dislocation tangles and pairs of intersecting twins, similar to that reported by Chen et al. [233]. The presence of crossing twins is evident from the SAED pattern in Figure 6.11c.

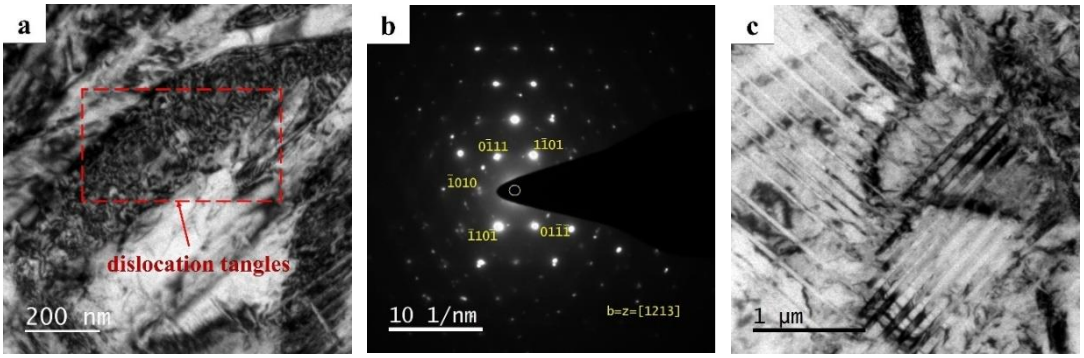

Figure 6.12 TEM images of USSP240 sample fatigue tested at ±0.70% strain amplitude having α′ laths with (a)dislocation tangles (b) SAED pattern along the [1$\bar{2}$1$\bar{3}$]α′ zone axis (c) twin-twin intersection.

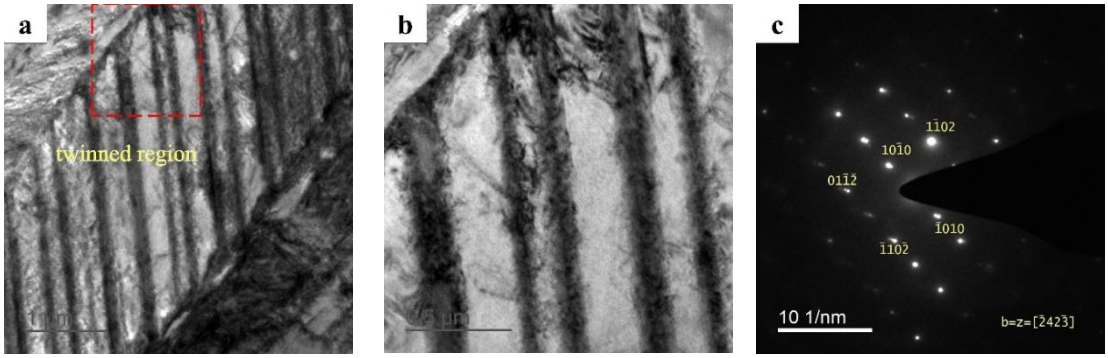

Figure 6.13 TEM images of USSP240-SR sample fatigue tested at ±0.70% strain amplitude having α′ laths (a)twinned region (b) enlarged view along with (c)SAED pattern along the [2$\bar{4}$2$\bar{3}$]α′ zone axis

The SAED pattern showed two types of twins; (1$\bar{1}$01)[1$\bar{1}$0$\bar{2}$] and (0$\bar{1}$11)[0$\bar{1}$1$\bar{2}$] type, which belongs to six crystallographic equivalent variants of {1$\bar{1}$01} twinning system. Williams et al. proposed that the twin of {1$\bar{1}$01} type in the primary martensite plate is generated due to the post transformation shear [289]. Figure 6.12a shows presence of dislocation tangles within α′ laths. Pair of intersecting twins were also visible in USSP240 treated fatigue samples (Figure 6.12c). Many authors have demonstrated that twinning is a preferred way of accommodating severe plastic strain [290,291]. TEM examination of the fatigue tested USSP240-SR samples revealed presence of needle-like

α′ martensite and plate-like twins between various shear bands. Figure 6.13 also shows twinned region in α′ laths.

6.7 DISCUSSION

6.7.1 Nanostructure Development

In the present investigation, the effect of ultrasonic shot peening was studied on microstructure and low cycle fatigue behaviour of the Ti-13Nb-13Zr alloy, heat treated at 900 °C for 1 h and quenched in water, with reduced modulus [292], which is important for bioimplant applications. No phase change was observed after the USSP240 treatment; though, there was decrease in volume fraction of the β phase, due to formation of strain-induced α′ martensite [235]. The TEM and XRD analyses clearly show formation of nanostructures in surface region of the specimens subjected to USSP240. Formation of a thick layer of ultrafine grains, resulting from ultrasonic shot peening of the Ti-6Al-4V alloy has been reported earlier [86,135]. There was development of equiaxial nanograins with a large misorientation angle in the surface region, and associated with high strain [227]. In Figure 4.5, the selected area electron diffraction pattern displays nano grain rings as well as dispersed spots from a few coarse grains. The cumulative impact of grain refinement, micro strain, and instrumental broadening caused widening of the XRD peaks (Figure 6.1). Since titanium alloys have fewer slip systems, the strain is first accommodated by twinning, which lowers the local stress inside the material during plastic deformation. Twinning emerges as dominant deformation process for hcp materials at room temperature [231–233]. Grain refining mechanism, according to Lu et al., consists of twin-twin interaction at the sub-micron level and twin-dislocation interaction at the nanometric level [234].

The XRD peaks were also widened, indicating that the surface microstructure had been refined to nanoscale. A significant number of twin systems are activated during USSP and twin-twin interaction occurs, that obstructs the migration of generated dislocations, and it results in accumulation of a large number of dislocations at twin boundaries. The microstructure gets refined into irregular shaped nanograins with significant misorientations, by formation of twins and interactions at the dislocation-twin interface, that gives rise to a continuous ring-type SAED pattern. Surface imperfections of various sizes occur during the USSP process, due to rapid impacts of steel shots, and cause significant surface roughness on the USSP treated samples.

Surface grain refinement and the accompanying compressive residual stresses enhance microhardness in the top surface region of the USSP treated specimen (Figure 4.8). The progressive decrease in microhardness down the depth of the USSP240-treated sample can be linked to a gradient microstructure with increasing grain size, from the top surface to the interior, consistent with the previous finding [127]. During the process of severe plastic deformation by USSP, the high strain rate rapidly generates dislocations, which multiply and enhance the material's work hardening. The hardness of the USSP treated samples is enhanced due to work hardening of the surface region and grain refinement.

6.7.2 Fatigue Behaviour

As the duration of the USSP treatment was increased from 240 to 360 s there was decrease in fatigue life of the samples (Table 6.2.). This decrease in LCF life of the USSP360 fatigue sample can be linked to the adverse effect of surface roughness and microcrack formation, owing to excessive work hardening from the longer USSP treatment. Relatively there is less increment in the LCF life of 120 s USSP treated sample,

which can be ascribed to less positive impact of the nanostructure and compressive residual stress compared to the more damaging stress concentration effect resulting from the increased surface roughness.

6.7.2.1 Cyclic Stress Response

The cyclic stress response shows mild hardening in all the samples during the initial cycles, varying with the condition, it could be due to increase in dislocation density with increase in loading cycles [293]. The Un-USSP and USSP240 treated samples, at high strain amplitudes, show mild hardening after ~50 and 70 cycles, respectively due to generation of large number of dislocations and twins. The interaction of these leads to substantial cyclic hardening. In the USSP240-SR samples, cyclic softening after the initial hardening, was due to reduction in twin boundaries and annihilation of dislocations, resulting from the stress-relieving treatment [294]. Dislocation tangles were observed in the Un-USSP samples, tested at the lower strain amplitudes, which led to high stress concentration at the grain boundaries. These dislocation tangles formed from the accumulation of dislocations, after small amount of deformation during the initial cyclic loading. The formation of deformation twins is most recognizable feature in hcp materials, like titanium [295]. During initial loading cycles, plastic strain was firstly accommodated by deformation twins and a few slip systems.

Ti alloys have shown better strength due to the barrier action of the twin boundaries to dislocation movement, as well as improved uniform elongation due to twin-induced plasticity effect [296]. Fatigue crack propagation is believed to be delayed primarily by deflection of crack path and dampening effects at the twin boundaries [297]. Deformation-induced twin boundaries function as strong barriers to dislocation movement, causing stress localization along the twin boundaries, which may slow down

the progression of fatigue cracks. The presence of twins can be seen in all the samples. Pairs of crossing or intersected twins have been reported in the bi-modal Ti55511 titanium alloy [233].

Lee et al. [298] and Kobayashi et al. [299] have shown various phase transformations during different annealing temperatures of Ti-13Nb-13Zr alloy. During annealing the metastable α′ martensite tends to decompose into stable α and β phases due to the thermal equilibrium. The separation of α′ and α is difficult through XRD as both have same hcp structure. Nevertheless, it is rationale in terms of thermodynamics that α phase increases with increase in annealing temperature/ time, also this phase is harder than the α′ martensite [214]. A significant shift in stress level of the USSP240-SR specimens towards higher side, in the cyclic stress response curve, in respect to the Un-USSP and USSP240 specimens is due to increase in yield strength after annealing at 400°C [300]. Also, there is oxygen enrichment in surface region of the USSP240-SR samples which also contributes to increase in the stress response. The increase in strength is accompanied by decrease in ductility which results in poor fatigue resistance [301]. Microcracks form easily during cyclic loading in high strength titanium alloys, enriched with oxygen, having high notch sensitivity [302]. The formation of titanium oxide, could not be detected by XRD because of very low volume fraction. Oxygen penetrates rapidly in the USSP treated samples during stress-relieving due to the developed nanostructure which increases the reactivity [303]. Fukai et al. have also shown marked reduction in fatigue strength due to oxygen enrichment [301].

The surface roughness of the sample plays a vital role on fatigue life, as fatigue cracks are known to arise from surface of the sample. In general, for high fatigue life, surface roughness should be as minimal as possible. As the surface roughness increases

the effective compressive residual stresses decreases by creating stress concentration factors [241]. Regardless of the fact that the surface roughness of the USSP240 samples was increased, the associated nanostructured surface layer and accompanying high compressive residual stress suppressed the negative effects of the surface roughness. The fatigue life of the USSP240-SR samples is slightly reduced due to relieving of the associated compressive residual stresses in the surface region. In the USSP240-SR sample, the harmful effect of surface roughness comes into play and it reduces the fatigue life to some extent. The SEM fractographs in Figure 6.9 of the Un-USSP, USSP240, and USSP240-SR specimens, assessed at equivalent strain amplitudes, demonstrates a significant variation in inter-striation spacing. The more closely spaced striations and tortuousness of the crack propagation path indicate greater resistance against fatigue crack propagation. The number density of crack initiation sites follows the sequence Un-USSP>USSP240-SR>USSP240 specimen on the fractographs in Figure 6.8, implying that the USSP240 treated samples had the highest fatigue life compared to the other conditions. Because fatigue fractures are known to initiate from slip bands at the surface, the process of fatigue crack initiation from the surface of the USSP240 treated specimen is likely to have been delayed owing to surface nano structuring. Also, the crack has propagated to a larger depth before catastrophic failure in the USSP240 treated samples compared to the USSP240-SR samples as shown in Figure 6.8(g-h).

The initiation of cracks from inside, in the USSP240 treated specimens, can be noticed clearly in Figure 6.8(d-f). Similar type of initiation of cracks was found in nanocrystalline titanium, low carbon steel and copper [230,304,305]. The reason for the subsurface crack initiation in the case of titanium and copper has been attributed to the hardened surface layer and the surface compressive residual stresses formed during the surface modification process. The surface compressive residual stresses, generally

induced during USSP240, can act as the closure stress for the short fatigue cracks and also constrain the plastic deformation developing at the crack tip. In case of the high strength steel the hard intermetallic compounds are reported to be responsible for the subsurface crack initiation [304]. However, in the present study, no inclusions were noticed at the crack initiation sites of the USSP240 treated fatigue samples. Our investigation of the USSP240 treated fracture sample showed that the crack initiation site shifts inside with decrease in the strain amplitude. The crack initiation from inside the sample occurred only in the USSP240 treated specimens, with nanostructured surface layer. The non-uniformity of microstructure between the nanostructured layer and the substrate gives rise to local stress concentration, which causes crack initiation. The surface compressive residual stresses move the crack initiation site to inner portion of the samples, where fatigue behaviour is mainly related to the microstructural changes such as the grain size and spacing between the lamellar grains. Therefore, the enhanced fatigue life in the USSP240 treated fatigue samples may be associated with the crack initiation from inside of sample.

From all the fractographs a different nature of fracture is demonstrated, depending on the initial condition of the sample and the strain amplitudes. There is substantial enhancement in fatigue life of the USSP240 specimens, over the entire range of strain amplitudes, compared to the Un-USSP samples, which is due to collective effect of the surface grain refinement, and the associated compressive residual stresses. A reduction in fatigue life is obvious due to decrease in the magnitude of the near surface compressive residual stress in case of the USSP240-SR samples and there was mainly the effect of grain refinement. Further, while the compressive residual stresses at the surface may suppress surface crack initiation, the usually brittle surface oxide layers formed during exposure to high temperatures may promote it [303].

6.8 CONCLUSIONS

The following conclusions are drawn from this chapter:

1. Cyclic hardening was observed after 100 cycles in the Un-USSP and USSP240 treated samples while there was cyclic softening in the USSP240-SR samples.
2. In the USSP240, there was a threefold increase in low cycle fatigue life compared to the Un-USSP condition, with sub-surface crack initiation due to a mixed overall positive effect of nano-structuring and the associated compressive residual stresses in the surface region.
3. Improvement in fatigue life can also be observed in the USSP240-SR samples, although it was less (2.5 times) compared to the USSP240 samples due to reduced surface compressive residual stresses. The surface grain refinement in the USSP240-SR samples improved fatigue life as compared to the Un-USSP condition.
4. Subsurface crack initiation was observed in the USSP240 fatigue fracture specimens unlike the Un-USSP and USSP240-SR conditions in which crack initiation was observed from the surface.
5. The principal mode of deformation in fatigue tested samples was deformation twinning and dislocation slip due to limited number of slip systems in the alloy.